Dyes and Pigments 94 (2012) 459–468

Contents lists available at SciVerse ScienceDirect

Dyes and Pigments

journal homepage: www.elsevier.com/locate/dyepig

Theoretical studies on spectroscopic properties of ruthenium sensitizers absorbed to TiO_2 film surface with connection mode for DSSC

Jie Chen [a], Fu-Quan Bai [a], Jian Wang [a], Li Hao [a], Zai-Feng Xie [a], Qing-Jiang Pan [b,**], Hong-Xing Zhang [a,*]

[a] State Key Laboratory of Theoretical and Computational Chemistry, Institute of Theoretical Chemistry, Jilin University, Changchun 130023, People's Republic of China
[b] Key Laboratory of Functional Inorganic Material Chemistry of Education Ministry & Laboratory of Physical Chemistry, School of Chemistry & Materials Science, Heilongjiang University, Harbin 150080, People's Republic of China

ARTICLE INFO

Article history:
Received 17 October 2011
Received in revised form
19 January 2012
Accepted 19 January 2012
Available online 11 February 2012

Keywords:
Dye-sensitized solar cell
Density functional theory
Frontier molecular orbital
Absorption spectrum
TiO_2 surface model
Deprotonation

ABSTRACT

Electron injection from a photoexcited chromophore into the surface of mesoscopic semiconductor TiO_2 nanoparticles is one of the key electron transfer processes for DSSC. A reasonable and reliable TiO_2 surface model (dropped down the anatase (101) and rutile (110) crystals a slab model) was designed, which was employed to investigate the absorption behavior of the adsorbed dye molecules such as **C101**, **J13** and **N749** under DFT method. According to the calculation results, the detailed orbital components and absorption transition are obtained; furthermore, the ultrafast, excited-state electron injection and emission electron injection can be discriminated. Generally, both the connecting surfaces of TiO_2 and degree of deprotonating dye molecules could influence absorption spectrum intensely. Our calculations show that the more efficient DSSCs should have larger conjugation degree for ancillary ligands or the whole system, which is beneficial to photon absorption from the visible to near-IR region.

1. Introduction

Considering the environmental issue and renewable resources, more and more attentions are paid to the solar energy utilizations. Due to the unique advantages of the dye-sensitized solar cells (DSSCs), such as low cost and highly efficient conversion of sunlight into electricity [1–4], the attention to the DSSCs has risen to a well altitude and relentless efforts are underway on its development. And sensitizer molecules as seen as the core in DSSCs have been widely investigated and improved. And, as compared to those metal-free organic dyes [5–8] and non-ruthenium metal dyes [9–12], the highest energy conversion efficiency (up to 14%) under standard (Global Air Mass 1.5) illumination was only achieved by using Ru-containing dyes, among which the successful examples should be **N3**, **N719**, **N749** (black dye) and their derivatives [13–17]. Up to now, **N3** and closely related analogues are still research hotspot and improved deeply [18–20]. Our group has calculated and analyzed several typical Ru-centered complexes, such as **N749** [Ru (4, 4′, 4″-tricarboxy-2, 2′:6′, 2″-terpyridine) $(NCS)_3]^{4-}$, **C101** [Ru (4, 4′-bis(5-hexylthiophen-2-yl)-2, 2′-bipyridine) (4, 4′-carboxylicacid-4′-2, 2′-bipyridine) $(NCS)_2$] and **J13** [Ru (N-(4-Butoxyphenyl)-N-2-pyridinyl-2-pyridinamine) (4, 4′-carboxylicacid-4′-2, 2′-bipyridine) $(NCS)_2$], respectively [21]. Generally, the ligands of sensitizers derived from **N3** can be divided into three classes, anchoring, ancillary and NCS ligands, according to their function. The NCS ligands popularly afford hole for regenerative dyes [22], while anchoring ligands such as carboxylic groups are necessary to attach to the surface of TiO_2 film and facilitate the charge injection into the conduction band (CB) of TiO_2, so the 4,4′-carboxylicacid-4′-2,2′-bipyridine (**dcbpy**) is widely assembled for Ru dyes.

Titanium dioxide in nanocrystalline form is most thermodynamically stable with the (101) face dominating more than 94% and (110) face almost for the rest of the crystal surface. TiO_2 absorbs in the ultraviolet spectrum, but can be photosensitized by the adsorption of chromophores that, when excited, inject electrons into the TiO_2 conduction band. The properties of TiO_2 surfaces have been the subject of a wide range of theoretical studies. So far, numerous attempts have made to investigate those processes including the interaction between dye molecules and TiO_2 surface and charge injection mechanism [23–39]. A time-dependent density-functional theory (TD-DFT) study by De Angelis et al. [40] suggested that the charge-transfer mechanism may change from nonadiabatic to adiabatic as a result of proton transfer from the dye

* Corresponding author.
** Corresponding author.
E-mail addresses: panqj@yahoo.com.cn (Q.-J. Pan), zhanghx@mail.jlu.edu.cn (H.-X. Zhang).

0143-7208/$ – see front matter © 2012 Elsevier Ltd. All rights reserved.
doi:10.1016/j.dyepig.2012.01.018

to the surface. But the intelligible data of photoelectric properties are not obtained because the system is too complex and enormous. There were still very few studies concerned with the adsorption of larger carboxylic acid molecules to provide a better model of the chromophore–surface interaction, mainly due to the dual limits of scale and accuracy for simulations. Therefore, one of the aims of this paper is to model the adsorption of **C101**, **J13** and **N749** on TiO_2 surface, respectively, and to study its effect on the electronic structure of TiO_2 efficaciously. Based on this reasonable model, we could get the credible charge distribution and spectrum data, and assign the absorption character and the possible way of electronic injection, such as ultrafast and reduced-sensitizer injection [41]. Furthermore, the optimal model which can facilitate the efficiency of DSSC can be figured out.

2. Computational details

In this work, dye molecules are dissymmetrical, so C_1 symmetry was adopted to settle the conformation of each one of **C101**, **J13** and **N749** in ground state with different degree of deprotonation. They were fully optimized using DFT with the B3LYP functional (Becke's three parameter functional and the Lee-Yang-Parr functional) [42]. On the basis of such calculations, spectroscopic absorption of dyes with films was obtained by TDDFT [43] method. The polarizable continuum model (PCM) [44] was employed to simulate the solvent effects of acetonitrile solvent molecules. In recent year, TDDFT methods have been successfully used to calculate the singlet–singlet state and singlet–triplet state [45] transitions in many reports. Therefore, on the basis of optimized ground state

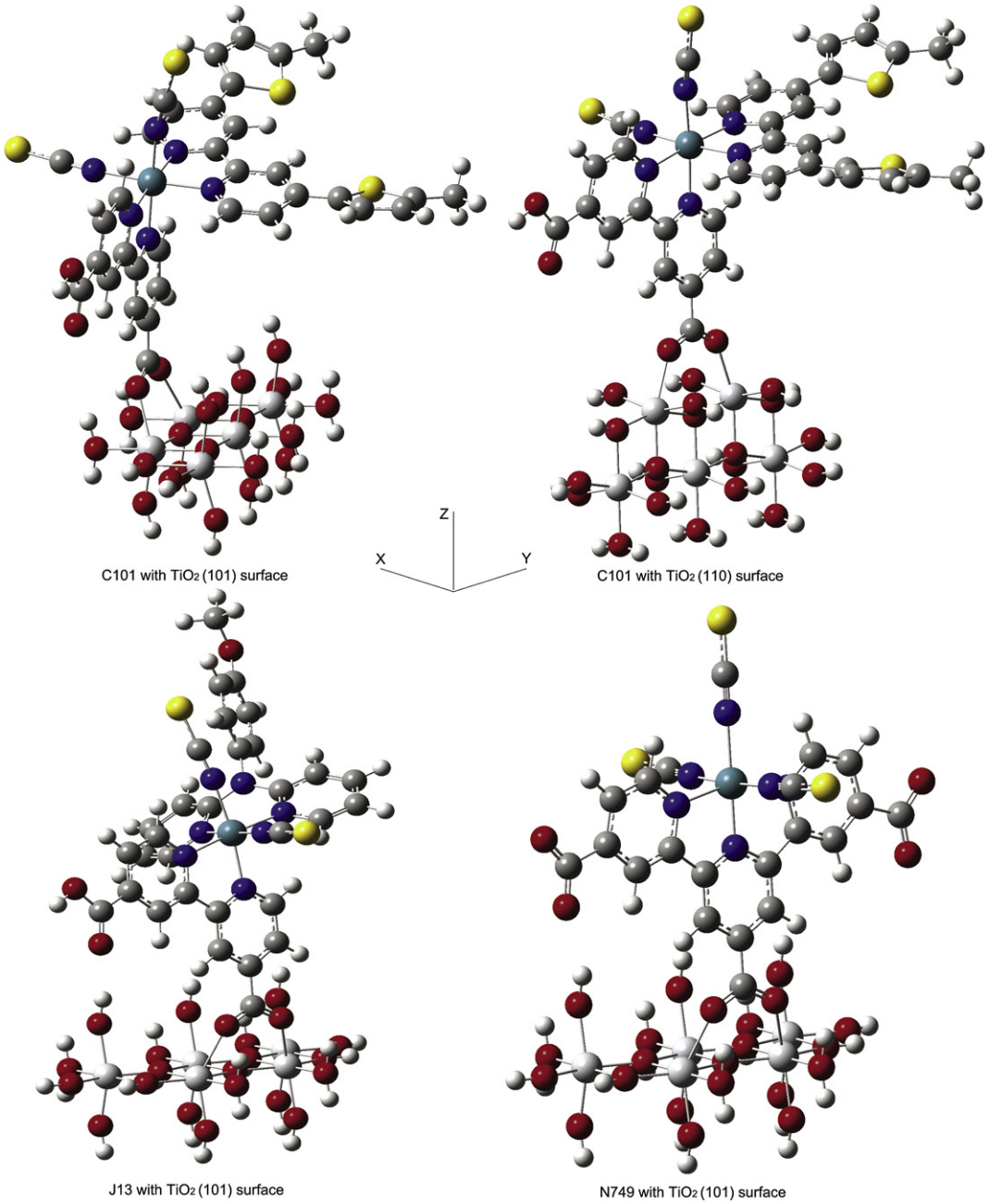

Fig. 1. Structures of dye molecules connected to different surfaces of TiO_2 film by TD-B3LYP.

geometry at B3LYP level of theory, we employed the TD-B3LYP method to calculate the absorptions. All UV/Vis spectra showed in the current discussed system were reflected with Gaussian curves of full-width at half-maximum (FWHM) of 1500 cm^{-1}.

In the calculations, quasi-relativistic pseudopotential of the Ru and Ti atoms proposed by Hay and Wadt [46] with respective 16 and 4 valence electrons was employed, and the LanL2DZ basis sets associated with the pseudopotential were adopted and a split valence basis set (6-31G*) was used to describe other atoms. Here, the basis sets were taken as Ru (8s7p6d/6s5p3d), Ti (8s7p6d1f/6s5p3d1f), S (16s10p1d/4s3p1d), O (10s5p/3s2p), and H (4s/2s). Thus, 1190-1188 basis functions and 622 electrons for **C101** (**1H-0H**) with TiO_2 (101) film, 1186-1184 basis functions and 622 electrons for **C101** (**1H-0H**) with TiO_2 (110) film, and 1138 basis functions and 586 electrons for **J13** (**2H**) with TiO_2 film etc., were included in the calculations. All calculations were accomplished by using the Gaussian09 (Revision A.02) program package [47].

3. Results and discussion

3.1. The structures for our nanoparticle models

3.1.1. An adopted models for TiO_2 film

As the semiconductor charge-transfer material, the choice of TiO_2 model is vital important for the DSSC efficiency. The TiO_2 slabs were generated from the optimized bulk geometry exposing the most thermodynamically stable surface: (110) in the case of rutile and (101) in the case of anatase.

And there are various connection types between dye molecules and TiO_2 film [48,49]. In fact, the connection types could be controlled by pH of the device systems, the surface of nanocrystalline, dye molecules and so on. Generally, the monodentate ester-type is the most basic connection model. In **N3** system, monodentate ester-type can form two steady single-bond connections with TiO_2 film [50]. But in **C101** system, the remarked degree of deprotonation is **1H**, moreover, the saturation strategy is adopted in **N749** system, so the number of carboxylic group side for connection is only one [51,52]. There are not reasonable about two steady single-bond connections in our systems, In addition, the characteristic of one monodentate ester-type is whirling, and the steady configuration is not exclusive. Furthermore, if it is appropriate, the other contiguous O atom may connect to TiO_2 with covalence bonded or weak interaction. In other words, the monodentate ester-type is a transition state; the absorptions for this type are weak and capricious. The bindentate chelating type is not steady in pure (101 or 110) surface as the strong tension. In fact this kind of type is dominant and descripted in TiO_2 cluster models [53]. There are steady bindentate chelating types at the edge of our adopted TiO_2 surface (at four-coordinated Ti atom), but in strictly speaking, this connective surface situation is between 101 and 110. So we deem that this type is not typical enough and not adopted in this work. At last bindentate bridging type is appropriate in this work. The bindentate bridging type is firm, which is the most important connection type in our systems for the strength and absorption efficiency. In this contribution, we only chose bindentate bridging type within the consideration for connection mode and suitable distance for binding.

Essentially, we have attempted many modes in various scales (from Ti_5 to Ti_{20}), and find out that the contributions of these scales to absorption were, in fact, not equivalent. In view of the effect of orbital coupling, those Ti atoms connected directly with **dcbpy** should make the most tremendous contribution to charge-transfer process, which afford primary transition-orbitals in absorption (*vide infra*). Identically, for the other Ti atoms, if they can afford conjugated orbits with connecting Ti, the certain degree of contribution will appear. And it could be concluded that the distance from Ti atom to the anchoring ligand **dcbpy** becomes the key factor. In other words, small scale models are reasonable in simulated calculation, which was also applied in other publication [54].

Finally, $Ti_5O_{20}H_{22}$ (101) and $Ti_5O_{20}H_{20}$ (110) models from crystal structures is adopted as surface of TiO_2 film in current work. As the

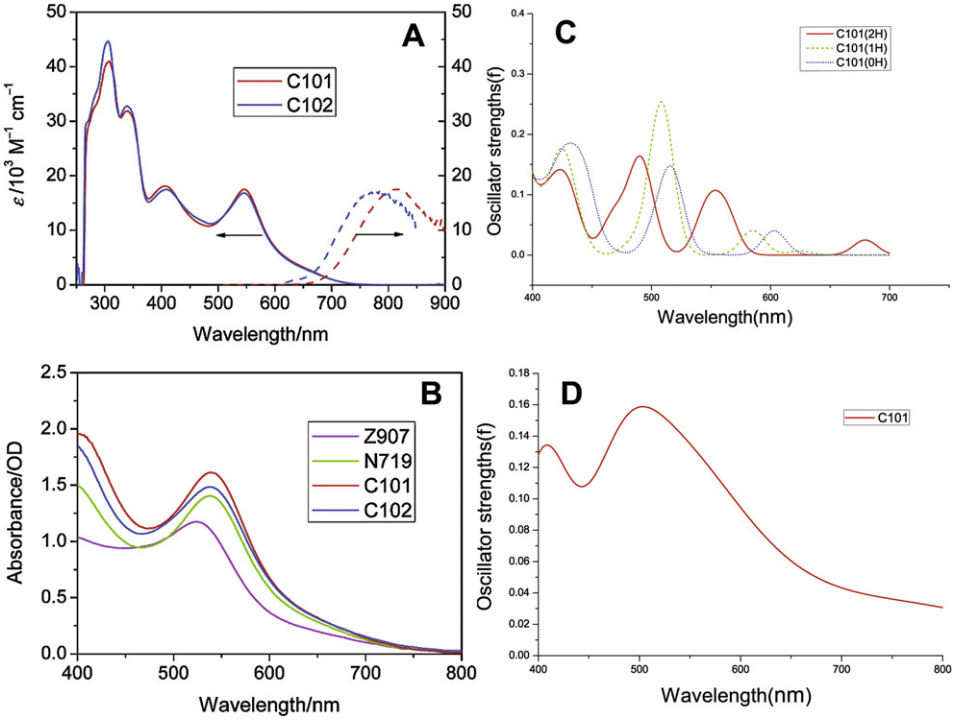

Fig. 2. Computational simulated absorption spectra of **I** system (right) and measured in experiment (left) from references [50]. (A) and (C) are about **C101** alone, while (B) and (D) are about dye molecule with TiO_2 film.

model is small enough that the large basis set (6-31G*) can be adopt in calculation. In this model, H atoms are for saturating the covalent bond of O atoms, and this method not only maintains bond-orientation in crystal, but also avoids the chaos of charge and multiplicity in the whole system. According to the scale of our model we selected the anatase (101) and rutile (110) surface, a single carboxyl-titanium dioxide connection (Fig. 1) was adopted to simulate the DSSC microcosmic surface charge-transfer transition.

3.1.2. The structures of the whole system

The full DFT optimizations on the dye complexes indicate that all of the complexes have an A symmetry ground state. And they show a pseudo-octahedral coordination for the Ru6N core, because the Ru (II) atoms adopt the low-spin $4d^6 5\ s^0$ electronic configuration. Anchoring ligand and one NCS ligand are nearly coplanar, so anchoring ligand-Ru-$N_6C_1S_1$ moiety lies on the *xy* plane and the other NCS ligand is slightly tilted with respect to the *z* axis.

In a simple Dewar, Chatt, and Duncanson model [55], the bond interaction can be described as a donation from a σ molecular orbital of the ligand (i.e., CN^- or NCS^-) toward an empty d orbital of metal and a concurrent back-donation from a filled (or partially filled) d orbital to a π^* antibonding orbital of the ligand. The two processes can promote and strengthen each other. Because of the polypyridine ligands have σ-donating orbitals localized on N atom, and π-donating or π^*-accepting orbitals delocalized on aromatic rings, back-donation between Ru and the π^* orbitals is significant [56].

Then, we linked one pyridine to TiO_2 mode and optimized the structure but with the TiO_2 moiety being set to frozen in Gaussian. According to the calculation about (101) surface, the bond length of O and Ti atoms between dye and film is about 2.17 Å, which is longer than that in crystal structure (1.93 or 1.97 Å). And the distance of carboxyl and pyridine is slight longer when **dcbpy** connected to film surface. Compared with (101) surface, there are not distinct differences about connective structure of (110) surface.

After that, the joint geometric parameters of pyridine and TiO_2 film are kept, and pyridine was replaced by the whole dye molecule (**C101**, **J13** and **N749**). Here, we considered that TiO_2 film have little influence to the most structure of dye molecules, if the distance is large enough. As so far as now, we can not get complete optimized-configuration, because of the limitations of calculation capacity. Even so, it is considered that this method is reasonable, because the joint section is not strong enough to change the configuration of dye, which is almost maintained by conjugation between Ru and ligands. And the calculated absorption curve of **C101** and **C101** with TiO_2 (101) surface in the calculation and experiment is shown in Fig. 2, which could be seen as the feasibility of our research. For **C101** monomer, the differences between experiment and simulation are not obvious. Concretely, the excited states of **1H** situation of **C101** arise the absorptions principally are referred to LUMO and LUMO+1 at 410 and 510 nm, with oscillator strength 0.1287 and 0.2426 in acetonitrile. Compared with the strong absorptions at 420 and 540 nm in experiment in DMF [51], the 10–30 nm blue-shifts should be considered as the solvent effect. In adsorbing system, there is nearly 40 nm deviation around the 500 nm in calculated absorption. In fact, there are three reasons that decided the deviation. First, in different experiments, besides the solvent environment is not same [51,57,58], the transition energies based on the real device condition are only provided in DSSC. In this work, the acetonitrile solvent is adopted, as the polarity of which is moderate and compromise. And the acetonitrile is also the real DSSC condition, while DMF is used in **C101** experiment. Second, there is the limitation of the TiO_2 model selection. Generally, as the larger mode is chosen, the more unoccupied MOs from TiO_2 mode could be obtained. And this kind of absorption (most of them are long-wave absorption) would be strengthened in some sort. Moreover, the oscillator strength about this kind of absorption is faintish rifely, the influence is not significant. Third, the connective models are dominant and exclusive in experiment, and the bindentate type is considered as the primary model in these systems [49–51].

We have attempted to employ some kinds of functionals with different emphasis such as PBE, B3LYP and M06-2X to expect best results. Finally, the B3LYP is adopted in this work. First, compared with experimental data and calculated data, the B3LYP functional has provided the more proximate result than others; second, B3LYP is broadly used in all of the similar works. Furthermore, the reasonable result had been obtained in our previous work for similar (Ru) systems. So we deem that the current data is assuring, and for simple and clear, the data from other functions are not provided in this paper.

3.2. Absorption spectra

3.2.1. Electronic structures

Since the frontier molecular orbitals play a relevant role in electronic transition process, it is necessary to examine the nature of the

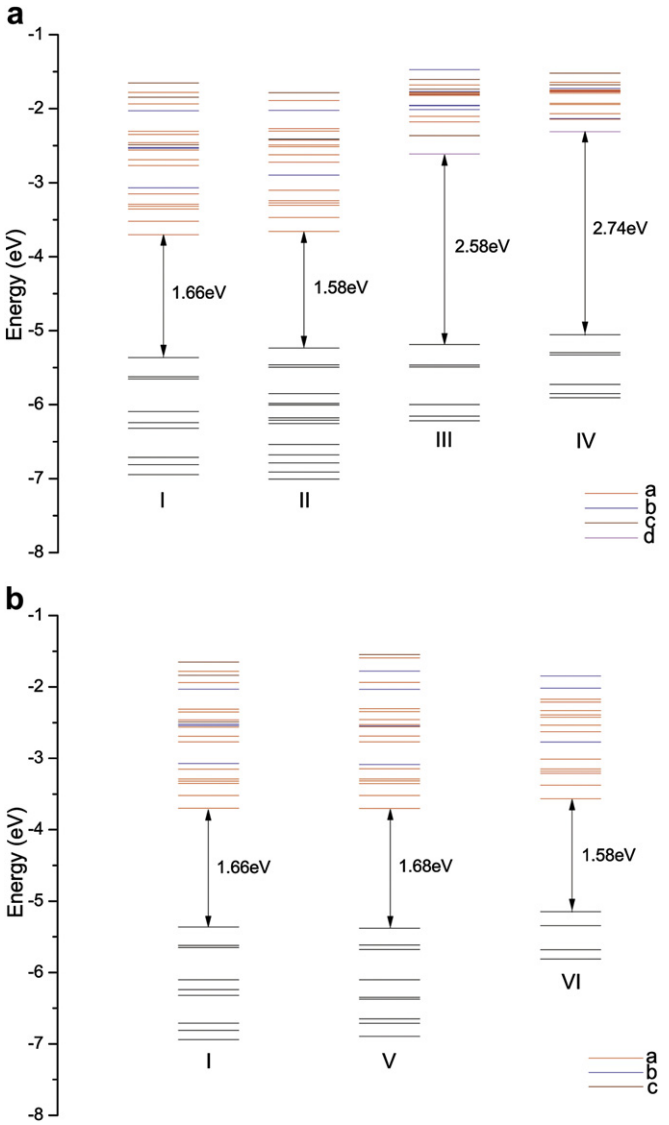

Fig. 3. Plot of the frontier molecular orbitals relevant to the absorptions for **I-VI** six systems in acetonitrile solution, calculated by the TDDFT method. (Especially, *a*: type means d orbital of Ti atoms; *b*: orbital mixed with Ti and anchoring ligands; *c*: orbital of ancillary ligands; *d*: type means orbital of anchoring ligands entirely.)

frontier molecular orbitals for these Ru (II) complexes under the framework for the excited-state TDDFT. The frontier molecular orbitals are plotted according to their energies and composition in Fig. 3 and detailed data are collected in Table 1 for system from **I** to **VI** (others shown in Table S3-6 in Supporting Information), where **I** is **C101** (**1H**) with TiO_2 (101); **II** is **C101** (**0H**) with TiO_2 (101); **III** is **C101** (**1H**) with TiO_2 (110); **IV** is **C101** (**0H**) with TiO_2 (110); **V** is **J13** (**1H**) with TiO_2 (101) and **VI** is **N749** (**0H**) with TiO_2 (101) film. We seek to understand the effect of deprotonation and connection fashion on absorption behavior of examined dyes, and their respective advantages and disadvantages are also shown in this paper.

The frontier molecular orbitals, which are responsible for absorption wavelength (λ) greater than 400 nm, are plotted according to their energies. Take **I** system as an example, the number of related unoccupied molecular orbitals (MOs) is more than that of occupied MOs. Specifically, there are twenty one unoccupied orbitals involved in the absorption process, as indicated in Table 1. Theoretical calculated some important orbitals are given in Fig. 4, most of which are contributed by d orbitals of Ti atoms. Due to the similar properties of occupied MOs for the different dye molecules [21,22] (for which the HOMO orbitals primarily lies on the anchoring ligand), we only need to pay attention to the unoccupied MOs. Concretely, electron cloud localized on the two connected Ti atoms from LUMO+0 to LUMO+4, and the followed higher energy unoccupied MOs contain the composition of other Ti atoms. In the term of distance factor, there are a few Ti atoms that are not included in this mode, but these atoms are coplanar with the connected Ti atoms, so the contribution would be negligible.

Until LUMO+6, the dominating orbital contribution from dye molecule is observed. Overall, there are only 5 of 21 orbitals that are not completely constituted by Ti atoms. Thus, when absorption happens, we deem that electrons was stimulated and entered into film directly, in other words, ultrafast, excited-state electron injection is the primary way of charge transfer that can be conducive to obtain the efficient DSSCs in practical application. Oppositely, if electrons injection does not occur at excited-state but when emission or sensitizer-reduction happens, it would result in long-time scale and low-utilization of solar [41].

When the degree of deprotonation increases about (101) surface system, the energies of anchoring and ancillary ligands rise slightly, leading to more components of unoccupied MOs from Ti atoms. In addition, the deprotonation system involves the orbital number is different from the aforementioned system, that the number of unoccupied MOs anticipating contribution reduce, while that of occupied MOs increase. But we could not get sufficient information about effect of deprotonation to absorption so far.

If dye molecules connect to TiO_2 film in (110) surface, energy levels would change notably. The related number of MOs decreases obviously, and the gap between HOMO and LUMO become tremendous. Furthermore, LUMO and LUMO+1 are contributed from the anchoring and ancillary ligand, respectively. Compared to (101) surface, the bond connected to dye owns more coordination ingredient, length of which is a little longer than that in crystal. Moreover, conjugated plane disappears in this situation. When the degree of deprotonation increased, the gap became larger. We tentatively come to conclude that (110) surface absorption would result in the increase in the whole energy of TiO_2 film, which affect against excited-state electron injection from dye molecules, which should be interpreted as the result of the electron injection of dye molecules into the CB of the TiO_2 film.

We simulated that different dye molecules absorbed to TiO_2 (101) surface, such as **C101**, **J13** and **N749**. Among them, both **C101**

Table 1
Partial molecular orbital Compositions (%) of **I** system in Acetonitrile. subscript [2] means the diploid *d* orbitals. (anch: anchoring ligands, anci: ancillary ligand, *: antibonding orbital).

I	Energy (eV)	Composition (%)						Assignment of orbital
MO		TiO_2	COO	anch	Ru	anci	NCS	
LUMO+20	−1.6509	8.3	0.8	5.6	1.5	83.2	0.5	π*(anci)
LUMO+19	−1.7799	72.6	3.4	13.3	0.8	9.7	0.3	d_{x2-y2}(Ti)[2]
LUMO+18	−1.8449	7.5	0.2	1.0	1.0	90.2	0.1	π*(anci)
LUMO+17	−1.9350	97.6	0.5	1.4	0.0	0.5	0.0	d_{yz}(Ti)[3]
LUMO+16	−2.0262	17.7	1.0	76.9	0.9	3.3	0.2	π*(anch)/d_{z2}(Ti)[2]
LUMO+15	−2.3065	99.4	0.5	0.1	0.0	0.0	0.0	d_{yz}(Ti)[3]
LUMO+14	−2.3467	98.7	1.2	0.1	0.0	0.0	0.0	d_{yz}(Ti)[2]/d_{yz}(Ti)[3]
LUMO+13	−2.4597	97.6	0.5	1.8	0.1	0.1	0.0	d_{xy}(Ti)[3]
LUMO+12	−2.4861	1.3	0.1	1.3	5.9	90.4	1.0	π*(anci)
LUMO+11	−2.5241	63.7	5.3	29.6	1.0	0.4	0.1	π*(anch)/d_{xz}(Ti)[3]
LUMO+10	−2.5361	65.4	4.8	28.3	1.1	0.3	0.1	π*(anch)/d_{xz}(Ti)[3]
LUMO+9	−2.5584	98.3	0.6	1.1	0.0	0.0	0.0	d_{yz}(Ti)[3]
LUMO+8	−2.6882	91.2	0.6	7.6	0.5	0.1	0.1	d_{yz}(Ti)[2]/d_{xy}(Ti)[3]
LUMO+7	−2.7682	99.3	0.5	0.1	0.0	0.0	0.0	d_{xz}(Ti)[2]/d_{xy}(Ti)[3]
LUMO+6	−3.0706	20.5	16.5	54.4	6.3	1.2	1.2	π*(anch)/d_{xy}(Ti)[2]
LUMO+5	−3.1489	97.8	1.6	0.6	0.0	0.0	0.0	d_{yz}(Ti)[2]/d_{xz}(Ti)[3]
LUMO+4	−3.2896	96.0	2.5	1.4	0.0	0.0	0.0	d_{x2-y2}(Ti)[2]
LUMO+3	−3.3174	98.7	0.9	0.4	0.0	0.0	0.0	d_{z2}(Ti)[2]
LUMO+2	−3.3541	96.2	1.6	1.9	0.2	0.0	0.0	d_{xy}(Ti)[2]
LUMO+1	−3.5215	94.3	3.0	2.2	0.3	0.0	0.0	d_{xz}(Ti)[2]
LUMO+0	−3.7043	98.4	1.5	0.2	0.0	0.0	0.0	d_{yz}(Ti)[2]
HOMO−LUMO Energy Gap								
HOMO−0	−5.3631	0.1	0.6	3.8	47.3	6.3	41.8	d_{xz}(Ru)-Π*(NCS)
HOMO−1	−5.6230	0.0	0.0	3.6	44.8	10.5	41.0	d_{yz}(Ru)-π*(NCS)
HOMO−2	−5.6538	0.1	0.1	5.3	41.5	3.4	49.6	d_{xy}(Ru)-π*(NCS)
HOMO−3	−6.0959	0.0	0.0	0.3	0.5	2.7	96.5	Π*(NCS)
HOMO−4	−6.2426	0.0	0.0	0.7	2.1	71.8	25.5	π(anci) π*(NCS)
HOMO−5	−6.3174	0.0	0.0	0.6	1.2	78.6	19.5	π(anci) π*(NCS)
HOMO−6	−6.7104	0.0	0.0	7.9	42.9	4.0	45.1	d_{xy}(Ru)-π*(NCS)
HOMO−7	−6.8105	0.0	0.1	3.2	41.2	20.7	34.8	d_{yz}(Ru)-π*(NCS)/π(anci)
HOMO−8	−6.9455	0.6	0.4	5.0	37.7	17.7	38.6	d_{xz}(Ru)-Π*(NCS)/π(anci)

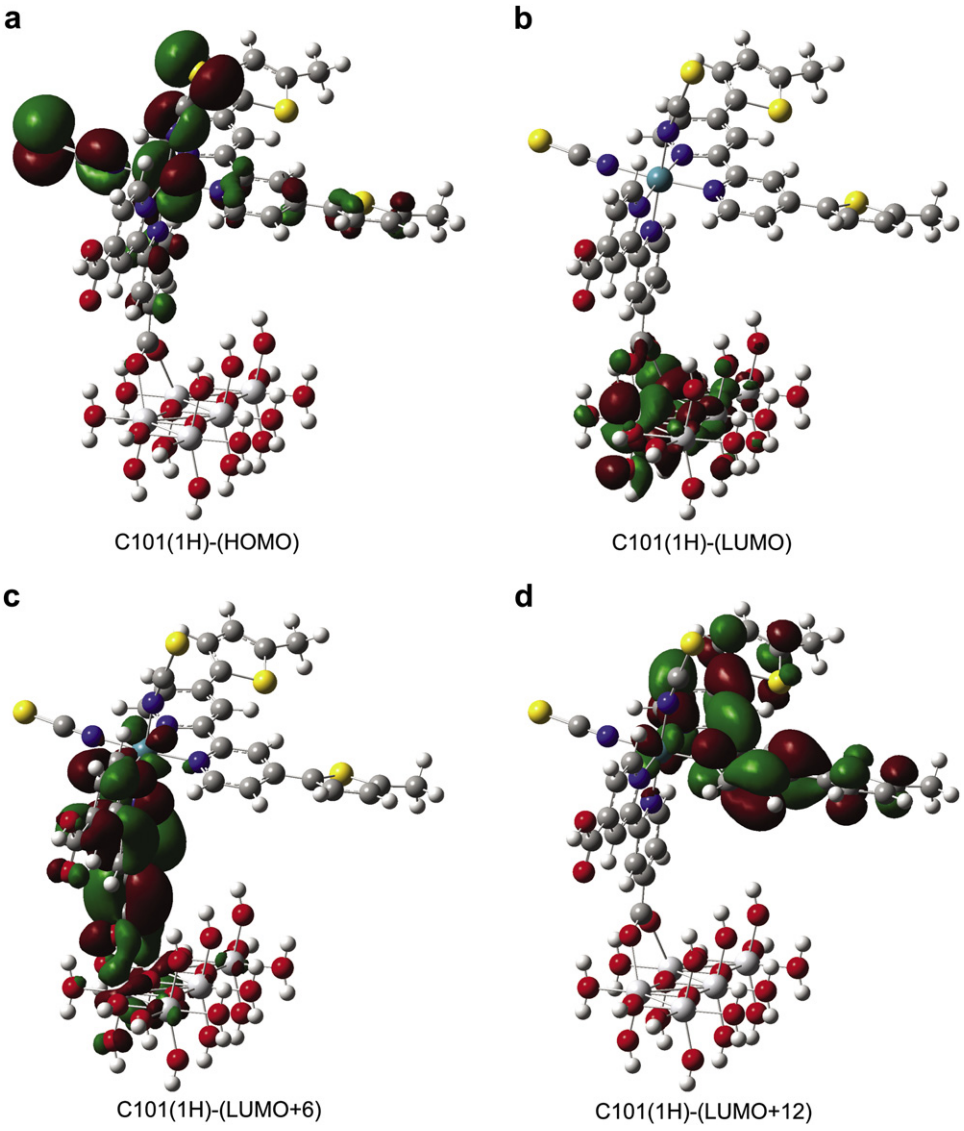

Fig. 4. Electron density diagrams of the frontier molecular orbitals relevant to the absorptions of **I** in acetonitrile media by TD-B3LYP. (isodensity surface is 0.02).

and **J13** belong to type of Ru (anchoring ligand) (ancillary ligand) $(NCS)_2$, so that the energy of occupied and unoccupied MOs are very similar. However, the arrangement of unoccupied MOs has some differences. Because of the non-conjugated property for the ligand of **J13**, its energy gap is relative higher than that of **C101**. Specifically, the lowest orbitals contributed by ancillary ligand are LUMO+19 for **J13** and LUMO+12 for **C101** system, respectively. For **N749** system with further degree of deprotonation, higher energy of occupied MOs is obtained. Meanwhile, the unoccupied MOs do not change distinctly, so the gap between HOMO and LUMO for highest degree of deprotonation is minimum, as indicated by our simulation. These properties could be favor of abundant absorption in long-wavelength region.

3.2.2. *Absorption spectra of **I**, **II**, **III** and **IV** in acetonitrile*

The absorption spectra of four systems in the acetonitrile solution are obtained by TD-B3LYP with PCM calculations. The calculated absorptions associated with their oscillator strengths (> 0.02), main configurations ($CI > 0.2$) and the character assignments for **I** system are summarized in Table 2. The fitted Gaussian-type absorption curves which are based on the calculated absorption data are shown in Fig. 5.

According to classification of different degree of deprotonation and connecting surface, it could be concluded that **C101** as an excellent dye molecule can bring about abundant absorption when $\lambda > 400$ nm, even in **III** and **IV** systems with enormous gap between HOMO and LUMO. Moreover, there is a distinct absorption peak near 400 nm in each system, and the characteristics of absorption are nearly all the same. Generally, the absorption spectra at this range could be assigned as the electron transfer from the contribution of d orbitals of Ru and π^* orbitals of NCS ligands to d orbitals of Ti and π^* orbitals of anchoring or ancillary ligands of dye molecule itself. Specifically, it is hard to discriminate the primary and secondary contribution for affording unoccupied MOs in each system, so the electron-transfer occurs not only from dye molecules to TiO_2 film, but also interior of dye molecules itself. In other words, this kind of charge-transfer would lead to both ultrafast, excited-state electron injection and emission electron injection.

For **I** system alone, there is an intense absorption peak concentrating on about 500 nm, and every important charge transition of which almost involves the LUMO+6 etc. in which all of them are consisted of both π^* orbitals of anchoring ligand and d orbitals of Ti atoms. In this range, the contribution of long-wavelength absorption has more relationship to the d orbitals of Ti atoms. And it would

Table 2
Calculated absorptions (λ > 400 nm) of **I**, **III**, **V** and **VI** systems in acetonitrile media by TD-B3LYP method. (anch: anchoring ligands; anci: ancillary ligandbonding orbital, *: anti bonding orbital).

	Peak	Enm (eV)	Oscillator strength	Config (CI coeff)	Assignment
I					
C101 (**1H**) with TiO_2 (101) surface	1	818.0(1.52)	0.0311	H-0→L+1(0.65)	d_{xz}(Ru)-Π*(NCS)→d_{xz}(Ti)[2]
				H-0→L+6(0.21)	d_{xz}(Ru)-Π*(NCS)→π*(anch)/d_{xy}(Ti)[2]
		679.6(1.82)	0.0265	H-2→L+1(0.65)	d_{xy}(Ru)-π*(NCS)→d_{xz}(Ti)[2]
				H-0→L+6(0.21)	d_{xz}(Ru)-Π*(NCS)→π*(anch)/d_{xy}(Ti)[2]
		625.7(1.98)	0.0256	H-2→L+2(0.63)	d_{xy}(Ru)-π*(NCS)→d_{xy}(Ti)[2]
				H-2→L+6(0.23)	d_{xy}(Ru)-π*(NCS)→π*(anch)/d_{xy}(Ti)[2]
		592.9(2.09)	0.0473	H-2→L+2(0.27)	d_{xy}(Ru)-π*(NCS)→d_{xy}(Ti)[2]
				H-2→L+6(0.58)	d_{xy}(Ru)-π*(NCS)→π*(anch)/d_{xy}(Ti)[2]
		560.6(2.21)	0.0347	H-0→L+12(0.63)	d_{xz}(Ru)-Π*(NCS)→π*(anci)
		546.4(2.27)	0.0835	H-0→L+8(0.37)	d_{xz}(Ru)-Π*(NCS)→d_{yz}(Ti)[2]/d_{xy}(Ti)[3]
				H-0→L+10(0.33)	d_{xz}(Ru)-Π*(NCS)→π*(anch)/d_{xz}(Ti)[3]
				H-0→L+11(0.33)	d_{xz}(Ru)-Π*(NCS)→π*(anch)/d_{xz}(Ti)[3]
		489.4(2.53)	0.1515	H-2→L+8(0.20)	d_{xy}(Ru)-π*(NCS)→d_{yz}(Ti)[2]/d_{xy}(Ti)[3]
				H-2→L+10(0.21)	d_{xy}(Ru)-π*(NCS)→π*(anch)/d_{xz}(Ti)[3]
				H-2→L+11(0.21)	d_{xy}(Ru)-π*(NCS)→π*(anch)/d_{xz}(Ti)[3]
				H-2→L+12(0.21)	d_{xy}(Ru)-π*(NCS)→π*(anci)
				H-1→L+12(0.53)	d_{yz}(Ru)-π*(NCS)→π*(anci)
		473.4(2.62)	0.0203	H-3→L+6(0.61)	Π*(NCS)→π*(anch)/d_{xy}(Ti)[2]
	2	414.1(2.99)	0.0476	H-7→L+1(0.46)	d_{yz}(Ru)-π*(NCS) π(anci)→d_{xz}(Ti)[2]
				H-0→L+18(0.45)	d_{xz}(Ru)-Π*(NCS)→π*(anci)
		413.0(3.00)	0.0323	H-7→L+1(0.45)	d_{yz}(Ru)-π*(NCS)/π(anci)→d_{xz}(Ti)[2]
				H-0→L+18(0.37)	d_{xz}(Ru)-Π*(NCS)→π*(anci)
		398.4(3.11)	0.0327	H-3→L+12(0.64)	Π*(NCS)→ π*(anci)
		397.8(3.12)	0.0256	H-8→L+1(0.32)	d_{xz}(Ru)-Π*(NCS) π(anci)→d_{xz}(Ti)[2]
				H-6→L+2(0.25)	d_{xy}(Ru)-π*(NCS)→d_{xy}(Ti)[2]
				H-6→L+4(0.21)	d_{xy}(Ru)-π*(NCS)→d_{x2-y2}(Ti)[2]
				H-6→L+6(0.31)	d_{xy}(Ru)-π*(NCS)→π*(anch)/d_{xy}(Ti)[2]
				H-0→L+20(0.35)	d_{xz}(Ru)-Π*(NCS)→π*(anci)
III					
C101 (**1H**) with TiO_2 (110) surface	1	579.6(2.14)	0.0409	H-1→L+0(0.23)	d_{yz}(Ru)-π*(NCS)→π*(anch)
				H-0→L+1(0.64)	d_{xz}(Ru)-Π*(NCS)→π*(anci)
		536.7(2.31)	0.1384	H-2→L+0(0.64)	d_{xy}(Ru)-π*(NCS)→π*(anch)
				H-1→L+1(0.20)	d_{yz}(Ru)-π*(NCS)→π*(anci)
		495.3(2.50)	0.1061	H-2→L+1(0.24)	d_{xy}(Ru)-π*(NCS)→π*(anci)
				H-1→L+1(0.58)	d_{yz}(Ru)-π*(NCS)→π*(anci)
		462.1(2.68)	0.0784	H-0→L+4(0.51)	d_{xz}(Ru)-Π*(NCS)→π*(anch)/d_{xz}(Ti)[5]
				H-0→L+6(0.34)	d_{xz}(Ru)-Π*(NCS)→π*(anch)/d_{xz}(Ti)[3]
	2	429.8(2.88)	0.0386	H-3→L+0(0.27)	Π*(NCS)→π*(anch)
				H-0→L+9(0.21)	d_{xz}(Ru)-Π*(NCS)→d_{xz}(Ti)[2]
				H-0→L+12(0.44)	d_{xz}(Ru)-Π*(NCS)→π*(anch)/π*(anci)/d_{xz}(Ti)[2]
				H-0→L+15(0.25)	d_{xz}(Ru)-Π*(NCS)→π*(anci)/π*(anch)/d_{xz}(Ti)[2]
		429.2(2.89)	0.0350	H-3→L+0(0.60)	Π*(NCS)→π*(anch)
				H-0→L+12(0.22)	d_{xz}(Ru)-Π*(NCS)→π*(anch)/π*(anci)/d_{xz}(Ti)[2]
		422.0(2.94)	0.0721	H-2→L+4(0.37)	d_{xy}(Ru)-π*(NCS)→π*(anch)/d_{xz}(Ti)[5]
				H-2→L+6(0.25)	d_{xy}(Ru)-π*(NCS)→π*(anch)/d_{xz}(Ti)[3]
				H-0→L+13(0.40)	d_{xz}(Ru)-Π*(NCS)→π*(anci)/d_{xz}(Ti)[2]
				H-0→L+15(0.22)	d_{xz}(Ru)-Π*(NCS)→π*(anci)/π*(anch)/d_{xz}(Ti)[2]
		420.1(2.95)	0.0377	H-2→L+4(0.38)	d_{xy}(Ru)-π*(NCS)→π*(anch)/d_{xz}(Ti)[5]
				H-2→L+6(0.26)	d_{xy}(Ru)-π*(NCS)→π*(anch)/d_{xz}(Ti)[3]
				H-0→L+13(0.41)	d_{xz}(Ru)-Π*(NCS)→π*(anci)/d_{xz}(Ti)[2]
		403.5(3.07)	0.0313	H-0→L+13(0.21)	d_{xz}(Ru)-Π*(NCS)→π*(anci)/d_{xz}(Ti)[2]
				H-0→L+15(0.44)	d_{xz}(Ru)-Π*(NCS)→π*(anci)/π*(anch)/d_{xz}(Ti)[2]
				H-0→L+16(0.40)	d_{xz}(Ru)-Π*(NCS)→π*(anch)/π*(anci)/d_{xy}(Ti)[5]
		395.6(3.13)	0.0454	H-3→L+1(0.67)	d_{yz}(Ru)-π*(NCS) π(anci)→ π*(anci)
V					
J13 (**1H**) with TiO_2 (101) surface	1	819.4(1.51)	0.0272	H-0→L+1(0.60)	d_{xz}(Ru)-Π*(NCS)→d_{xz}(Ti)[2]
				H-0→L+6(0.30)	d_{xz}(Ru)-Π*(NCS)→π*(anch)/d_{xy}(Ti)[2]
		546.5(2.27)	0.0908	H-0→L+8(0.36)	d_{xy}(Ru)-π*(NCS)→d_{yz}(Ti)[2]/d_{xy}(Ti)[3]
				H-0→L+10(0.46)	d_{xz}(Ru)-Π*(NCS)→π*(anch)/d_{xz}(Ti)[3]
	2	403.1(3.08)	0.0251	H-8→L+1(0.41)	d_{xz}(Ru)-Π*(NCS)→d_{xz}(Ti)[2]
				H-2→L+15(0.20)	d_{xy}(Ru)-Π*(NCS)→π*(anch)/d_{yz}(Ti)[2]
				H-0→L+19(0.35)	d_{xz}(Ru)-Π*(NCS)→π*(anci)

	Peak	Enm (eV)	Oscillator strength	Config (CI coeff)	Assignment	Exp (nm)
VI						
N749 (**0H**) with TiO_2 (101) surface	1	627.9(1.97)	0.1557	H-1→L+6(0.68)	d_{xz}(Ru)-Π*(NCS)→π*(anch)/d_{xy}(Ti)[2]	630
	2	502.7(2.47)	0.0209	H-1→L+14(0.69)	d_{xz}(Ru)-Π*(NCS)→π*(anch)	520
		493.4(2.51)	0.0360	H-1→L+11(0.22)	d_{xz}(Ru)-Π*(NCS)→d_{xy}(Ti)[2]	
				H-0→L+14(0.63)	d_{xy}(Ru)-Π*(NCS)→π*(anch)	
		465.9(2.66)	0.0463	H-5→L+6(0.69)	Π*(NCS)→π*(anch)/d_{xy}(Ti)[2]	

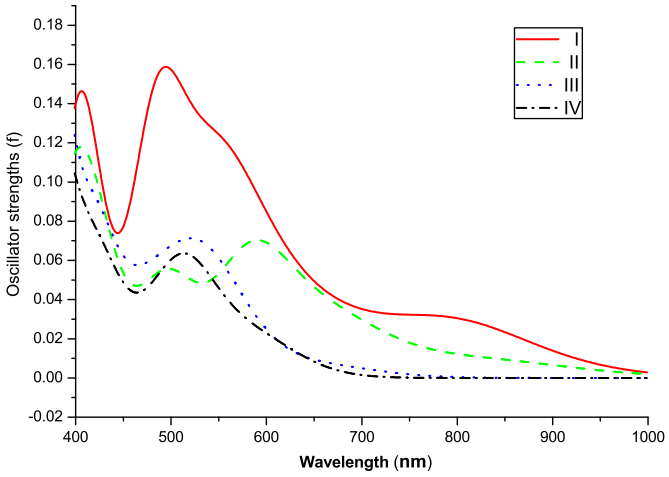

Fig. 5. Simulated absorption spectra of **I**, **II**, **III** and **IV** in acetonitrile media.

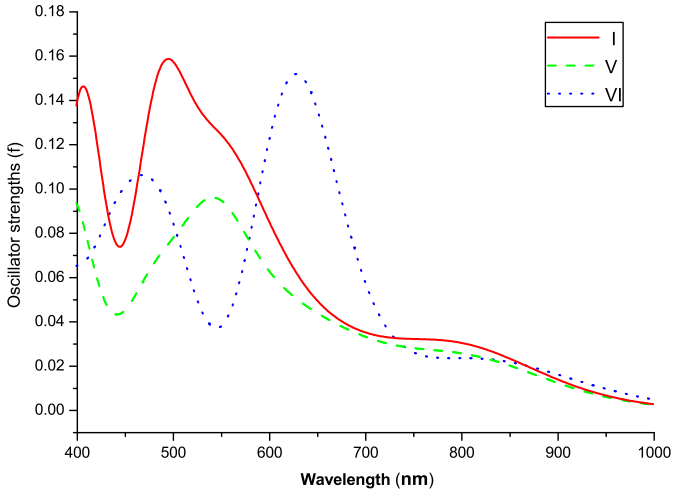

Fig. 6. Simulated absorption spectra of **I**, **V** and **VI** in acetonitrile media.

reduce as the wavelength shortened, thus, long-wavelength absorption benefits for ultrafast, excited-state electron injection in **I** system.

II system owns higher degree of deprotonation than **I**, and there are two particular absorption peaks: one is concentrated on about 600 nm, the other lies in the range of about 500 nm. The former has some relation to d orbitals of Ti in the film. The latter, however, only concern intermolecular charge transfer. Obviously, the absorption properties of **II** system are not as well as **I** system in DSSCs and the possible reason can be attributed to that the deprotonation could enhance the energy of orbital, which involves in anchoring ligand. Unfortunately, since energy matching to absorbing transition, several orbitals involving anchoring ligand are very important to long-wavelength absorption, such as LUMO+6, LUMO+11 and LUMO+12 in **I** system. But for **II** system, we only find LUMO+6 with higher energy. Finally, it could be seen that some small modulation such as degree of deprotonation would influence the integral efficiency of DSSCs enormously.

Essentially, longer-wavelength absorptions in both **III** and **IV** system lead to charge-transfer internally. Because there are not sufficient orbital-coupling, the absorption spectrum is similar to the dye molecule alone, which we have calculated in detail before. In fact, if dye molecules absorbed to the TiO_2 (110) surface, the orbital energy of TiO_2 is higher than dye molecule. Overall, this is the reason why the 110 surface of TiO_2 film is not chosen in practice.

3.2.3. *Absorption spectra of **IV** and **VI** in acetonitrile*

We selected three typical kinds of dye molecules connecting to the TiO_2 (101) surface and the integrated Gaussian-type absorption curves are shown in Fig. 6. Being dye molecules, **J13** and **N749** do not bring out abundant absorption as well as **C101**, when absorption $\lambda > 400$ nm. Specifically, the transition of absorption about **J13** with TiO_2 film is similar with **C101**, but oscillator strengths. In fact, the design purpose of **J13** is not achieved [57], and enhancing energy of ancillary ligands does not help to orbital-coupling.

VI system with relation to **N749** does not own complex absorption in visible region, but the oscillator strengths are distinguished. As the thorough saturated tactic is adopted in experiment, the connecting mode of bindentate type should be pure in **N749** system. Besides, the calculated absorptions are very close to the experimental values. There is only one notable peak near 630 nm in the same solvent environment (acetonitrile) [58], and the deviation is not exceeding 10 nm between experiment and calculation. This system is the only one that the absorption wavelength is red-shift obviously. Because of this, the utilization of red light is the highest in all six systems. The oscillator strengths of absorption near 630 nm are as well as that in **I** system near 500 nm, while the other absorption near 460 nm is weaker. So we deem that the total IPCE (incident photon to current conversion efficiency) of **I** system is higher than **VI** system. With higher symmetry, the conjugation of **N749** is strong. As a result the energy of **N749** is low, and the orbital-coupling is satisfactory, for which there are more mixed types of orbital than other systems. However, the disadvantage lies on the small contribution from d orbitals of Ti atoms, which is adverse effect on ultrafast, excited-state electron injection. The DSSCs that could utilize sunlight fully is the focus of research, so people pay much attention to **N749** as efficient dye molecule all the time. If the improvement is appropriate, the better DSSCs could be prepared.

4. Conclusions

Electronic structures and spectroscopic properties of several typical dye molecules which are absorbed to different TiO_2 film are investigated theoretically. Taking into account the deprotonation effect, the following conclusions can be drawn.

For different TiO_2 surface, as the ingredient of connecting bond of Ti atoms is not the same, there are great differences about absorption and energy levels, when the orbital-coupling happens. Generally, (110) surface is not good for charge injection. Moreover, the degree of deprotonation could influence the absorption in visible region extremely, because all of the active orbitals are affected during this process.

As the improvement of ancillary ligands, the thiophene group can enrich the absorption greatly. Though it is against ultrafast, excited-state electron injection, that the ancillary ligands participate in absorbing transition directly, the utilization of solar energy would still increase. In addition, the conjugation for the whole system can enhance the efficiency of DSSCs, such as **N749**.

For all of the six systems in this experiment, the LUMO+6 etc. that are delocalized on both TiO_2 film and anchoring ligands make a great contribution to absorption in the visible range. We suppose that the more efficient DSSC would be obtained, if the energy of these orbitals could be reduced, availably.

Acknowledgments

This work was supported by the Natural Science Foundation of China (Grant No. 20703015, 20973076, and 21003057) and Program

for New Century Excellent Talents in Heilongjiang Provincial University of China (1154-NCET-010) and Specialized Research Fund for the Doctoral Program of Higher Education (20110061110018).

Appendix. Supplementary material

Supplementary material associated with this article can be found, in the online version, at doi:10.1016/j.dyepig.2012.01.018.

References

[1] O'Regan B, Grätzel M. A low-cost, high-efficiency solar cell based on dye-sensitized colloidal TiO_2 films. Nature 1991;353:737–40.
[2] Hagfeldt A, Grätzel M. Molecular Photovoltaics. Acc Chem Rev 2000;33:269–77.
[3] Grätzel M. Photoelectrochemical cells. Nature 2001;414:338–44.
[4] Kalyanasundaram K, Grätzel M. Applications of functionalized transition metal complexes in photonic and optoelectronic devices. Coord Chem Rev 1998;177:347–414.
[5] Hara K, Sato T, Katoh R. Molecular design of Coumarin dyes for efficient dye-sensitized solar cells. J Phys Chem B 2003;107:597–606.
[6] Horiuchi T, Miura H, Sumioka K, Uchida S. High efficiency of dye-sensitized solar cells based on metal-free Indoline dyes. J Am Chem Soc 2004;126:12218–9.
[7] Pinheiro HM, Touraud E, Thomas O. Aromatic amines from azo dye reduction: status review with emphasis on direct UV spectrophotometric detection in textile industry wastewaters. Dyes Pigm 2004;61:121–39.
[8] Ito S, Zakeeruddin SM, Humphry-Baker R. High-Efficiency organic-dye-sensitized solar cells controlled by nanocrystalline-TiO_2 Electrode Thickness. Adv Mater 2006;18:1202–5.
[9] Kuciauskas D, Freund MS, Gray HB, Winkler JR, Lewis NS. Electron transfer Dynamics in nanocrystalline titanium dioxide solar cells sensitized with ruthenium or Osmium Polypyridyl complexes. J Phys Chem B 2001;105:392–403.
[10] Islam A, Sugihara H, Hara K, Singh LP, Katoh R, Yanagida M, et al. Dye sensitization of nanocrystalline titanium dioxide with Square Planar Platinum (II) diimine dithiolate complexes. Inorg Chem 2001;40:5371–80.
[11] Wang Q, Campbell WM, Bonfantani EE, Jolley KW, Officer DL. Efficient light Harvesting by using Green Zn-Porphyrin-Sensitized nanocrystalline TiO_2 films. J Phys Chem B 2005;109:15397–409.
[12] Geary EAM, Yellowlees LJ, Jack LA, Oswald IDH. Synthesis, structure, and properties of [Pt(II)(diimine)(dithiolate)] dyes with 3,3'-, 4,4'-, and 5,5'-disubstituted bipyridyl: applications in dye-sensitized solar cells. Inorg Chem 2005;44:242–50.
[13] Nazzruddin MK, Kay A, Rodicio I, Humphry-Baker R. Conversion of light to electricity by cis-X2bis(2,2'-bipyridyl-4,4'-dicarboxylate)ruthenium (II) charge-transfer sensitizers (X = Cl-, Br-, I-, CN-, and SCN-) on nanocrystalline titanium dioxide electrodes. J Am Chem Soc 1993;115:6382–90.
[14] Nazeeruddin MK, Zakeeruddin SM, Humphry-Baker R, Jirousek M, Liska P. Acid–Base Equilibria of (2,2'-Bipyridyl-4,4'-dicarboxylic acid)ruthenium (II) complexes and the effect of Protonation on charge-transfer sensitization of nanocrystalline Titania. Inorg Chem 1999;38:6298–305.
[15] Nazeeruddin MK, Pechy P, Renouard T, Zakeeruddin SM. Engineering of efficient Panchromatic sensitizers for nanocrystalline TiO_2-based solar cells. J Am Chem Soc 2001;123:1613–24.
[16] Komatsuzaki NO, Yanagida1 M, Funaki T, Kasuga K, Sayama K, Sugihara H. Near-IR dye-sensitized solar cells using a new type of ruthenium complexes having 2,6-bis(quinolin-2-yl)pyridine derivatives. Sol Energy Mater Sol Cells 2011;95:310–4.
[17] Baryshnikov GV, Minaev BF, Minaeva VA. Quantum-chemical study of effect of conjugation on structure and spectral properties of C105 sensitizing dye. Opt Spectrosc 2011;110:393–400.
[18] Jang SR, Choi MJ, Vittal R, Kim KJ. Anchorage of N3 dye-linked polyacrylic acid to TiO_2/electrolyte interface for improvement in the performance of a dye-sensitized solar cell. Sol Energy Mater Sol Cells 2007;91:1209–14.
[19] Dai FR, Wu WJ, Wang QW, Tian H, Wong WY. Heteroleptic ruthenium complexes containing uncommon 5,5'-disubstituted-2,2'-bipyridine chromophores for dye-sensitized solar cells. Dalton Trans 2011;40:2314–23.
[20] Ning ZJ, Fu Y, Tian H. Improvement of dye-sensitized solar cells: what we know and what we need to know. Energy Environ Sci 2010;3:1170–81.
[21] Li MX, Zhou X, Xia BH, Zhang HX, Pan QJ, Liu T, et al. Theoretical studies on structures and spectroscopic properties of photoelectrochemical cell ruthenium sensitizers, [Ru(Hmtcterpy)(NCS)3]n- (m) 0, 1, 2, and 3; n) 4, 3, 2, and 1). Inorg Chem 2008;47:2312–24.
[22] Nazeeruddin MK, De Angelis F, Fantacci S, Selloni A, Viscardi G, Liska P, et al. Combined experimental and DFT-TDDFT Computational study of photoelectrochemical cell ruthenium sensitizers. J Am Chem Soc 2005;127:16835–47.
[23] Qin P, Zhu HJ, Edvinsson T, Boschloo G, Hagfeldt A, Sun LC. Design of an organic chromophore for P-type dye-sensitized solar cells. J Am Chem Soc 2008;130:8570–1.
[24] Nilsing M, Lunell S, Persson P, Ojamae L. Phosphonic acid adsorption at the TiO_2 anatase (1 0 1) surface investigated by periodic hybrid HF-DFT computations. Surf Sci 2005;582:49–60.
[25] Nilsing M, Persson P, Ojamae L. Anchor group influence on molecule–metal oxide interfaces: periodic hybrid DFT study of pyridine bound to TiO_2 via carboxylic and phosphonic acid. Chem Phys Lett 2005;415:375–80.
[26] Persson P, Lundqvist MJ. Calculated Structural and electronic interactions of the ruthenium dye N3 with a titanium dioxide nanocrystal. J Phys Chem B 2005;109:11918–24.
[27] Lundqvist MJ, Nilsing M, Lunell S, Akermark B, Persson P. Spacer and Anchor Effects on the Electronic Coupling in Ruthenium-bis-Terpyridine Dye-Sensitized TiO_2 Nanocrystals Studied by DFT. J Phys Chem B 2006;110:20513–25.
[28] Persson P, Lundqvist MJ, Ernstorfer R, Goddard WA, Willig F. Quantum chemical calculations of the influence of Anchor-Cum-Spacer groups on Femtosecond electron transfer times in dye-sensitized semiconductor Nanocrystals. J Chem Theory Comput 2006;2:441–51.
[29] Nilsing M, Persson P, Lunell S, Ojamae L. Dye-Sensitization of the TiO2 rutile (110) surface by Perylene dyes: quantum-chemical periodic B3LYP computations. J Phys Chem C 2007;111:12116–23.
[30] Wolpher H, Sinha S, Pan JX, Johansson A, Lundqvist MJ, Persson P, et al. Synthesis and electron transfer studies of Ruthenium–Terpyridine-based Dyads Attached to Nanostructured TiO_2. Inorg Chem 2007;46:638–51.
[31] Barolo C, Nazeeruddin MK, Fantacci S, Censo DD, Comte P, Liska P, et al. Synthesis, Characterization, and DFT-TDDFT Computational study of a ruthenium complex containing a functionalized Tetradentate ligand. Inorg Chem 2006;45:4642–53.
[32] Ghosh S, Chaitanya GK, Bhanuprakash K, Nazeeruddin MK, Grätzel M, Reddy PY. Electronic structures and absorption spectra of Linkage Isomers of Trithiocyanato (4,4',4''-Tricarboxy-2,2':6,2''-terpyridine) Ruthenium(II) complexes: a DFT study. Inorg Chem 2006;45:7600–11.
[33] Nazeeruddin MK, Wang Q, Cevey L, Aranyos V, Liska P, Klein EC, et al. DFT-INDO/S modeling of New high Molar Extinction Coefficient charge-transfer sensitizers for solar cell Applications. Inorg Chem 2006;45:787–97.
[34] Lowry MS, Bernhard S. Synthetically Tailored excited states: Phosphorescent, Cyclometalated Iridium(III) complexes and their Applications. Chem-Eur J 2006;12:7970–7.
[35] Li JR, Nilsing M, Kondov I, Wang HB, Persson P, Lunell S, et al. Dynamical simulation of Photoinduced electron transfer Reactions in Dye–Semiconductor systems with different Anchor groups. J Phys Chem C 2008;112:12326–33.
[36] Hagberg DP, Marinado T, Karlsson KM, Nonomura K, Qin P, Boschloo G, et al. Tuning the HOMO and LUMO energy levels of organic chromophores for dye sensitized solar cells. J Org Chem 2007;72:9550–6.
[37] Qin H, Wenger S, Xu M, Gao F, Jing X, Wang P, et al. An organic sensitizer with a Fused Dithienothiophene Unit for efficient and stable dye-sensitized solar cells. J Am Chem Soc 2008;130:9202–3.
[38] Howie WH, Claeyssens F, Miura H, Peter LM. Characterization of Solid-state dye-sensitized solar cells utilizing high absorption Coefficient metal-free organic dyes. J Am Chem Soc 2008;130:1367–75.
[39] Tian HN, Yang XC, Chen RK, Zhang R, Hagfeldt A, Sunt LC. Effect of different dye Baths and dye-structures on the performance of dye-sensitized solar cells based on Triphenylamine dyes. J Phys Chem C 2008;112:11023–33.
[40] De Angelis F, Fantacci S, Selloni A, Nazeeruddin MK, Grätzel M. Time-Density functional theory Investigations on the excited states of Ru(II)-dye-sensitized TiO_2 nanoparticles: the role of sensitizer Protonation. J Am Chem Soc 2007;129:14156–7.
[41] Ardo S, Meyer GJ. Photodriven heterogeneous charge transfer with transition-metal compounds anchored to TiO_2 semiconductor surfaces. Chem Soc Rev 2009;38:115–64.
[42] Becke AD. Density-functional thermochemistry. III. The role of exact exchange. Chem Phys 1993;98:5648–52.
[43] (a) Casida ME, Jamorski C, Casida KC, Salahub DR. Molecular excitation energies to high-lying bound states from time-dependent density-functional response theory: characterization and correction of the time-dependent local density approximation ionization threshold. J Chem Phys 1998;108:4439–49;
(b) Stratmann RE, Scuseria GE. An efficient implementation of time-dependent density-functional theory for the calculation of excitation energies of large molecules. J Chem Phys 1998;109:8218–24;
(c) Matsuzawa NN, Ishitani A. Time-dependent density functional theory calculations of photoabsorption spectra in the vacuum ultraviolet region. J Phys Chem A 2001;105:4953–62.
[44] Tomasi J, Mennucci B, Cammi R. Quantum mechanical continuum solvation model. Chem Rev 2005;105:2999–3094.
[45] (a) Bauernschmitt R, Ahlrichs R. Treatment of electronic excitations within the adiabatic approximation of time dependent density functional theory. Chem Phys Lett 1996;256:454–64;
(b) Rosa A, Baerends EJ, Gisbergen SJ. Electronic spectra of $M(CO)_6$ (M = Cr, Mo, W) revisited by a relativistic TDDFT approach. J Am Chem Soc 1999;121:10356–65.
[46] (a) Wadt WR, Hay PJ. Ab initio effective core potentials for molecular calculations. potentials for main group elements Na to Bi. J Chem Phys 1985;82:284–98;
(b) Hay PJ, Wadt WR. Ab initio effective core potentials for molecular calculations.

Potentials for K to Au including the outermost core orbitals. J Chem Phys 1985;82: 299–310.
[47] Frisch MJ, Trucks GW, Schlegel HB, Scuseria GE, Robb MA, Cheeseman JR, et al. Gaussian 09, revision C.02. Wallingford CT: Gaussian, Inc.; 2009.
[48] Falaras P. Synergetic effect of carboxylic acid functional groups and fractal surface characteristics for efficient dye sensitization of titanium oxide. Sol Energy Mater Sol Cells 1998;53:163–75.
[49] Weng YX, Li L, Liu Y, Wang L, Yang GZ. Surface-Binding forms of carboxylic groups on Nanoparticulate TiO_2 surface Studied by the interface-sensitive transient triplet-state molecular Probe. J Phys Chem B 2003;107:4356–63.
[50] Persson P, Lunell S. Binding of bi-isonicotinic acid to anatase TiO_2 (1 0 1). Solar Energy Mater Solar Cells 2000;63:139–48.
[51] Gao FF, Wang Y, Shi D, Zhang J, Wang M, Jing XY, et al. Enhance the Optical Absorptivity of nanocrystalline TiO_2 film with high Molar Extinction Coefficient ruthenium sensitizers for high performance dye-sensitized solar cells. J Am Chem Soc 2008;130:10720–8.
[52] Lee GW, Kim D, Ko MJ, Kim K, Park NG. Evaluation on over photocurrents measured from unmasked dye-sensitized solar cells. Solar Energy 2010;84: 418–25.
[53] Guo ZY, Liang WZ, Zhao Y, Chen GH. Real-Time Propagation of the reduced one-electron density Matrix in atom-centered orbitals: application to electron injection Dynamics in dye-sensitized TiO_2 Clusters. J Phys Chem C 2008;112: 16655–62.
[54] Syres K, Thomas A, Bondino F, Malvestuto M, Grätzel M. Dopamine adsorption on anatase TiO_2(101): a Photoemission and NEXAFS Spectroscopy study. Langmuir 2010;26:14548–55.
[55] Chatt A, Duncanson JL. Olefin co-ordination compounds. Part III. Infra-red spectra and structure: attempted preparation of acetylene complexes. J Chem Soc; 1953:2939.
[56] Boulet P, Chermette H, Daul C, Gilardoni F, Rogemond F, Weber J, et al. Absorption spectra of several metal complexes Revisited by the time-dependent density-functional theory-response theory formalism. J Phys Chem A 2001;105:885–94.
[57] Jin ZZ, Masuda H. Triarylamine-Functionalized ruthenium dyes for efficient dye-sensitized solar cells. ChemSusChem 2008;1:901–4.
[58] Katoh R, Furube A, Kasuya M, Fuke N, Koide N, Han L. Photoinduced electron injection in black dye sensitized nanocrystalline TiO_2 films. J Mater Chem 2007;17:3190–6.